Am J Physiol Renal Physiol 295: F60–F72, 2008.
First published May 7, 2008; doi:10.1152/ajprenal.00618.2007.

VEGF receptors and neuropilins are expressed in the urothelial and neuronal cells in normal mouse urinary bladder and are upregulated in inflammation

Marcia R. Saban,[1] Joseph M. Backer,[2] Marina V. Backer,[2] Julie Maier,[3] Ben Fowler,[3] Carole A. Davis,[1] Cindy Simpson,[1] Xue-Ru Wu,[5] Lori Birder,[4] Michael R. Freeman,[6] Shay Soker,[7] Robert E. Hurst,[8] and Ricardo Saban[1]

[1]*Department of Physiology, University of Oklahoma Health Sciences Center, Oklahoma City;* [2]*SibTech, Incorporated, Brookfield, Connecticut;* [3]*Oklahoma Medical Research Foundation, Imaging Core Facility, Oklahoma City;* [4]*Department of Medicine, University of Pittsburgh School of Medicine, Pittsburgh, Pennsylvania;* [5]*Department of Urology, New York University Medical School, New York, New York;* [6]*Departments of Urology, Surgery, and Biological Chemistry and Molecular Pharmacology, Children's Hospital Boston, Harvard Medical School, Boston, Massachusetts;* [7]*Wake Forest Institute for Regenerative Medicine, Wake Forest University School of Medicine, Winston-Salem, North Carolina; and* [8]*Departments of Urology, Biochemistry, and Molecular Biology, University of Oklahoma Health Sciences Center, Oklahoma City, Oklahoma*

Submitted 28 December 2007; accepted in final form 1 May 2008

Saban MR, Backer JM, Backer MV, Maier J, Fowler B, Davis CA, Simpson C, Wu X-R, Birder L, Freeman MR, Soker S, Hurst RE, Saban R. VEGF receptors and neuropilins are expressed in the urothelial and neuronal cells in normal mouse urinary bladder and are upregulated in inflammation. *Am J Physiol Renal Physiol* 295: F60–F72, 2008. First published May 7, 2008; doi:10.1152/ajprenal.00618.2007.—Recent evidence supports a role for vascular endothelium growth factor (VEGF) signaling in bladder inflammation. However, it is not clear what bladder cells are targeted by VEGF. Therefore, we determined the nature of cells responding to VEGF in normal and inflamed bladders by tagging such cells in vivo with a targeted fluorescent tracer, scVEGF/Cy, an engineered single-chain VEGF labeled with Cy5.5 dye, which identifies cells with accessible and functionally active VEGF receptors. Inflammation was induced by intravesical instillation of PAR-activating peptides or BCG. In vivo NIRF imaging with intravenously injected scVEGF/Cy revealed accumulation of the tracer in the control mouse bladder and established that inflammation increased the steady-state levels of tracer uptake. Ex vivo colocalization of Cy5.5 dye revealed that in normal and at a higher level in inflamed bladder, accumulation of scVEGF/Cy occurs in both urothelial and ganglial cells, expressing VEGF receptors VEGFR-1 and VEGFR-2, as well as VEGF coreceptors neuropilins (NRP) NRP1 and NRP2. PCR results indicate that the messages for VEGF-Rs and NRPs are present in the bladder mucosa and ChIP/QPCR analysis indicated that inflammation induced upregulation of genes encoding VEGFRs and NRPs. Our results strongly suggest new and blossoming VEGF-driven processes in bladder urothelial cells and ganglia in the course of inflammation. We expect that molecular imaging of the VEGF pathway in the urinary tract by receptor-mediated cell tagging in vivo will be useful for clinical diagnosis and therapeutic monitoring, and will help to accelerate the development of bladder-targeting drugs and treatments.

bladder inflammation; VEGF coreceptors; interstitial cystitis; VEGF receptor imaging; human urothelium; targeted imaging; scVEGF/Cy fluorescent tracer; Cy5.5

RECENT EVIDENCE PLACES vascular endothelium growth factor (VEGF) signaling in the center of molecular pathways underlying urinary tract inflammation. In normal bladder this signaling is a key mechanism downstream of protease-activated receptor (PARs) activation in response to proinflammatory stimuli (36, 40), while in bladder with the superficial cancer it is part of the response to intravesical therapy with Bacillus Calmette-Guerin (BCG) (34). This new appreciation of VEGF's signaling role in bladder inflammation is supported by emerging evidence that levels of various VEGF proteins are, in general, increased at the site of inflammation (20, 26, 27, 35, 49) and that infiltrating lymphocytes and other inflammatory cells represent an additional source of VEGF (24, 27). However, it is not clear what bladder cells are targeted by VEGF and which VEGF's functions are important in the rather harsh bladder environment. Although the "traditional" VEGF targets are endothelial cells in vascular and lymphatic systems, recent evidence indicates more diverse targets/functions for this growth factor.

As VEGF and its receptors participate in the responses of the bladder to inflammation, we wished to establish the nature of cells expressing VEGF receptors and coreceptors in normal and inflamed bladders and to develop a methodology for assessing VEGF signaling in vivo. Although the "usual suspects" vascular and lymphatic endothelial cells are the target of VEGF signaling in many normal and diseased tissues, expression of VEGF receptors by bladder cancer cells (15, 33) suggested that the situation might be different or, at least, more complex in this organ. To answer this question experimentally, we chose to use two different stimuli that have been proven to induce significant and reproducible bladder inflammation and alter VEGF signaling upon intravesical instillation, namely protease-activated receptors activating peptides (PAR-APs) (39, 41) and BCG (37).

To identify cells with accessible and functionally active VEGF receptors, we tagged such cells in vivo with a new, internalizable fluorescent tracer, scVEGF/Cy (10), and then used immunohistochemical markers to characterize the lineage of tagged cells. The tracer is based on a single-chain (sc)

Address for reprint requests and other correspondence: R. Saban, College of Medicine, Univ. of Oklahoma Health Sciences Center (OUHSC), Urinary Tract Physiological Genomics Laboratory, 800 Research Parkway, Rm. 410, Oklahoma City, OK 73104 (e-mail: ricardo-saban@ouhsc.edu).

The costs of publication of this article were defrayed in part by the payment of page charges. The article must therefore be hereby marked "*advertisement*" in accordance with 18 U.S.C. Section 1734 solely to indicate this fact.

Table 1. *Primary antibody characteristics*

Antigen	Host Species	Against	Dilution	Code	Supplier	Address
AUM (uroplakin polyclonal)	Rabbit	Bovine AUM	1:10,000		Dr. X-R Wu (50, 51)	
Neuronal specific enolase	Rabbit (P)	Human	1:200	ab16873	Abcam	www.abcam.com
Neuropilin 1	Goat (P)	Mouse	1:750	24-6800	eBioscience	www.ebioscience.com
Neuropilin 1 (a1 CUB domain)	Rabbit	Human	1:100	NP2111	ECM Biosciences	www.ecmbiosciences.com
Neuropilin-1 (a1 CUB Domain) Blocking Peptide		Human	10 mg/ml	NX2115	ECM Biosciences Zymed	www.ecmbiosciences.com
Neuropilin-2	Rabbit	Human (NH_2-term)	1:100	36-1500	Zymed Laboratories, Inc.	South San Francisco, California 94080
Vascular endothelium growth factor-R1 (Flt-1)	Rabbit	Human (COOH-term)	1:50	RB-9049	NeoMarkers	www.labvision.com
Vascular endothelium growth factor-R2 (Flk-1)	Rat	Mouse	1:50	550549	BD Pharmingen	
CD31	Rat	Mouse	1:50	550274	BD Pharmingen	
LYVE-1	Rabbit	Mouse	1:400	ab14917	Abcam	www.abcam.com

VEGF that was constructed by fusing two fragments (amino acids 3-112) of VEGF121 lacking proangiogenic COOH-terminal domain and expressed with the NH_2-terminal cysteine-containing tag (Cys-tag) for site-specific conjugation of therapeutic and diagnostic payloads (8–10). scVEGF/Cy is prepared by site-specific conjugation of the near-infrared fluorescent dye, Cy5.5 to Cys-tag in scVEGF, and functional activity of the tracer is comparable to that of parental VEGF in tissue culture assays, such as induction of VEGFR-2 tyrosine autophosphorylation, competition with a VEGF toxin for binding to cellular VEGFR-2, and VEGFR-mediated internalization (9). In several mouse tumor models, VEGF receptor-mediated internalization of intravenously injected scVEGF/Cy but not a control inactive tracer (inVEGF/Cy) resulted in selective long-term accumulation of Cy5.5 in the tumor, particularly at the tumor periphery and contiguous host vasculature, as established by noninvasive near-infrared fluorescent imaging of whole animals and fluorescent microscopy of histological sections (10). Importantly, unlike immunohistochemical analysis that shows all cells expressing VEGF receptors, receptor-mediated tagging with scVEGF/Cy tracer identifies only cells with accessible and functionally active VEGF receptors (8–10).

We report here that urothelial and ganglial cells in the mouse urinary bladder express VEGFRs and neuropilins (NRPs) that are primarily responsible for uptake of scVEGF/Cy tracer. Finally, in experimental bladder inflammation, there is an enhanced accumulation of scVEGF/Cy in the same cells suggesting that they are important targets for VEGF signaling.

MATERIALS AND METHODS

Experimental Bladder Inflammation

All animal experimentation described here was performed in conformity with the APS *Guiding Principles in the Care and Use of Animals* (4), and the animal protocol 05-088I was approved by the OUHSC Animal Care & Use Committee protocol (IACUC). Ten- to 12-wk-old C57BL/6 female and male mice (Jackson Laboratory, Bar Harbor, ME) were used in this research. Female mice were anesthetized, transurethrally catheterized as previously described (37), and instilled on *days 1*, *7*, *14*, and *21* with 200 μl of one of the following substances: pyrogen-free saline ($n = 20$), BCG [TheraCys-Aventis-Pasteur; total dose of 1.35 mg (37)], control-inactive peptide [10 μM; LRGILS (32)], PAR1-AP [10 μM; SFFLRN (32)], and PAR2-AP [10 μM; SLIGRL (32)]. The efficacy of PAR-APs at a concentration of 10 μM (39) and BCG (37) at a concentration of 1.35 mg to induce bladder inflammation was determined previously. Mice were studied 24 h after a single instillation (saline and BCG acute) or 7 days after 4 weekly instillations (saline chronic, control peptide chronic, PAR1-AP chronic, PAR2-AP chronic, and BCG chronic).

Near-Infrared Fluorescent Imaging

Mice were fed a low-chlorophyll diet for 2 wk to reduce autofluorescence in the intestinal region (48) and the abdominal

Table 2. *Mouse primers used for PCR and ChiP-Q-PCR*

Gene	Alternative Name	Accession	Forward	Reverse
Q-PCR Primers				
NRP1		BC060129	ATGGGAAGCGAATCTGTAGG	CCAGGTCAAATGGAAATGAAAG
NRP2 precursor		AF022854	tgctatcttttgggggtttg	ggaccagttaccgcagagag
VEGFR1	Flt1	NM_010228	gggtcacacctcatctttctc	atgcaaaaggaagcccacta
VEGFR2	Flk-1	X70842	ggcagaccaagagcatctgt	gtttgggccgtgattctaaa
VEGFR3	Flt4	NM_008029.2	GGTTCATGGGAAAGGACTTG	gcaggacgagccattttatc
Untr6			TCAGGCATGAACCACCATAC	AACATCCACACGTCCAGTGA
PCR primers				
NRP1		BC060129	TGGGAAGATTGCACCTTCTCCTGT	TTGGTTTCCTTGGAAATGGCACCC
NRP2 precursor		AF022854	TGATTGGCAAGTACTGTGGGACGA	TTGAACTTGCGTACAAACGCCCTG
VEGFR1		NM_010228	TCTACAGCACCAAGAGCGATGTGT	TATCTTCATGGAGGCCTTGGGCTT
VEGFR2		X70842	GCTTGCCTTATGATGCCAGCAAGT	AAGAACTCCATGCCCTTAGCCACT

hair was removed. Mice were anesthetized with isoflurane and intravenously injected via the tail vein with 100 μl of ~0.5 nmol of the following substances: *1*) active tracer (scVEGF/Cy); or *2*) inactive tracer (inVEGF/Cy) prepared by biotinylation of 6–8 amino groups in scVEGF/Cy to prevent binding to VEGF receptors (10). Anesthetized mice were immediately placed on a heating pad inside a FluorChem HD2 cabinet (Alpha Innotech, San Leandro, CA) equipped with a Chromalight multi-wavelength illuminator with a Cy5 excitation filter (620 ± 60 nm) and images were captured with 4-megapixel cooled camera (F2.8 28- to 70-mm zoom lens) with a Qdot 705 emission filter (705 ± 10 nm). The FluorChem HD2 was coupled to a dedicated computer and images were first acquired and stored with AlphaEase FC 32-bit software (Alpha Innotech).

The FluorChem cabinet permits continued anesthesia with isoflurane and, therefore, accumulation of Cy5.5 fluorescent tracer was followed over time. Between 330 and 1,440 min (24 h), mice were returned to their respective cages. Following near-infrared fluorescent imaging (NIRF), mice were euthanized with pentobarbital sodium (100 mg/kg ip) and tissues were removed rapidly and frozen for immunofluorescence and ChIP-Q-PCR.

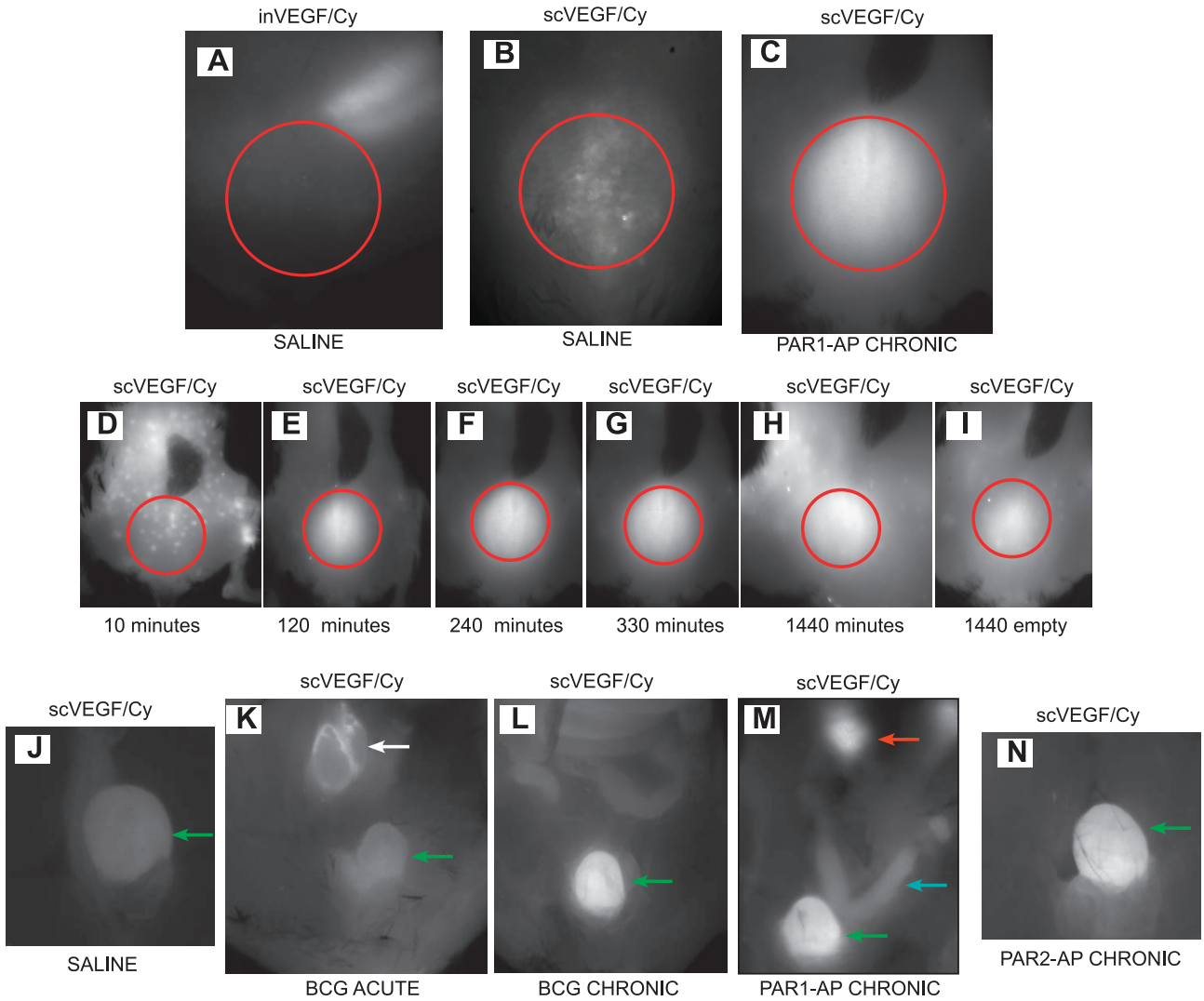

Fig. 1. In vivo visualization of scVEGF/Cy by near-infrared fluorescent imaging (NIRF). Mice were fed a low-chlorophyll diet for 2 wk to reduce autofluorescence in the intestinal region and the abdominal hair was removed. Mice were anesthetized with isofluorane and injected in the tail vein with 100 μl of scVEGF/Cy containing ~0.5 nmol of the tracer. Anesthetized mice were immediately placed on a heating pad inside a FluorChem HD2 (Alpha Innotech) equipped with a Chromalight multiwavelength illuminator with a Cy5 excitation filter (620 ± 60 nm) and images were captured with 4-megapixel Cooled camera (F2.8 28- to 70-mm zoom lens) with a Qdot 705 emission filter (705 ± 10 nm). The FluorChem HD2 was coupled to a dedicated computer and images were first acquired and stored with AlphaEase FC 32-bit software (Alpha Innotech). *A*: representative photograph of a group treated intravesically with saline that was injected intravenously at *time 0* with inVEGF/Cy in the tail vein and photographed at *time* 240 min. *B*: representative photograph of a group treated with saline intravesically that was injected intravenously at *time 0* with scVEGF/Cy in the tail vein and photographed at *time* 240 min. *C*: representative photograph of the observed fluorescence in the lower abdominal region of a mouse chronically treated with PAR1-AP that was injected intravenously at *time 0* with scVEGF/Cy in the tail vein and photographed at *time* 240 min. *D–I*: representative photographs of the observed fluorescence in the lower abdominal region of a mouse chronically treated with PAR1-AP that was injected at *time 0* with scVEGF/Cy in the tail vein. The numbers in each segment indicate the actual time lapse (minutes) after intravenous administration of scVEGF/Cy. Additional mice were euthanized 24 h after injection with scVEGF/Cy in the tail vein and had their abdomen opened and the gastrointestinal tract removed to permit a better visualization of the pelvic area. *J*: control (instillation of saline); *K*: acute instillation with BCG; *L*: chronic BCG treatment; *M*: PAR1-AP chronic treatment group; and *N*: PAR2-AP chronic treatment group. Outside the urinary bladders (green arrows), fluorescence was observed at its highest concentration in the kidneys (red arrows), lymph sacs draining the lower abdomen (white arrows), and uterus (blue arrow).

NIRF Image Analysis

NIRF image analysis was performed, as described recently (38). Briefly, images were first acquired and stored with AlphaEase FC 32-bit software (Alpha Innotech) and, subsequently Adobe Photoshop CS3 extended (1) that permitted the determination of integrated density. For this purpose, an elliptical marquee of fixed size (180 × 180 px) was used to determine the region of interest (ROI) around the luminescence zones corresponding to a bladder area, and the count tool was used to determine and record each integrated density. The integrated density corresponded to the sum of the values of the pixels in the ROI, which were equivalent to the product of the area (in pixels) and mean gray value.

Human Bladders

The same urothelial specimens that were collected for our previous study (46) were used in the present work. Samples were obtained from five controls and as previously described; informed consent was obtained from each patient. Five female patients with an average age of 46.1 years (range 21 to 66), known to be free of bladder mucosal disease and urinary tract infection, were undergoing a bladder suspension procedure for stress urinary incontinence and underwent bladder biopsy used for immunohistochemical analysis.

Immunofluorescence of Human and Mouse Tissues

Bladder tissue was processed for routine immunohistochemistry according to published methods (21, 41). Frozen sections were postfixed in 1% formaldehyde and all reagent incubations and washes were performed at room temperature. Five percent normal donkey blocking serum (Jackson Immunolabs) was placed on all slides for 45 min and sections were incubated with primary antibody for 1 h and 45 min in a humidified chamber. Slides were washed 3× 5 min in PBS and incubated with secondary antibodies. Slides were washed, counterstained with DAPI (1:20,000 dilutions of 10 mg/ml) for 2 min, and coverslipped with Shur/Mount (TBS) mounting media and sealed with nail polish. All tissue sections were visualized using a Zeiss Axiovert 200M inverted fluorescent microscope and imaged at room temperature using a Zeiss axiocam HRm high-resolution CCD camera, driven by Axiovision 4.6 software. Selected sections were visualized and photographed using a Zeiss LSM510 laser scanning confocal with META (Thornwood, NY). Controls included omission of the primary antibody. Antibodies used in this work included uroplakin provided by Wu et al. (50) and commercially available antibodies are listed on Table 1. All secondary antibodies were used at a 1:400 dilution and included donkey anti-rabbit IgG AF488 conjugate (Molecular Probes; probes.invitrogen.com), donkey anti-goat IgG (Alexa Fluor 546, A11056, Invitrogen), and donkey anti-rat IgG (AlexaFluor 488; used for VEGF-R2).

Image Analysis

At least six random fields per cross-section were visualized at ×200 magnification (if viewing Cy5.5 fluorescence, ×400 magnification was used) and used for image analysis that was performed with the NIS-Elements Advanced Research 2.3 imaging software (6). This software identifies signal by thresholding key intensity values. Furthermore, the software permits imposing restrictions to the measurements by excluding false positive signals. Briefly, the number of positive cells expressing a particular antibody was calculated as percent of the ROI, as indicated in the individual figure legend. Colocalization of fluorescence for one antibody and Cy5.5 or for two antibodies was calculated by converting the area occupied by cells positive for the first antibody into a ROI. Then, the percent of cells that were positive for the second antibody was calculated within the ROI. Results are expressed as means ± SE. In all cases, a value of $P < 0.05$ was considered indicative of a significant difference (12).

NRPs and VEGFRs PCR in the Mouse Bladder

Immediately after removal from the animal, bladders were placed in RNA*later* (Ambion) and visualized under a dissecting microscope (Nikon SMZ 1500). The urothelium and submucosa layers were separated by blunt dissection away from the detrusor muscle (43). Total RNA was extracted from the urothelium/submucosa in Ultraspec RNA solution (Biotecx Laboratories, Houston, TX) according to the manufacturer's instructions. The amount and quality of the RNA were verified by measuring the absorbance at 260 and 280 nm, and by electrophoresing the samples on a formaldehyde/agarose gel. Oligo(dT)-primed reverse transcription of RNA was performed with the SuperScript First-Strand Synthesis System for RT-PCR (Invitrogen, Carlsbad, CA), using 5 μg of RNA for each reaction. Following reverse transcription, PCR amplifications were performed from 2 μl of each cDNA. Primer pairs were designed using Primer 3 (3). The designed primers shared 100% homology with the target sequence but no significant homology with other sequences and primer sequences are listed in Table 2.

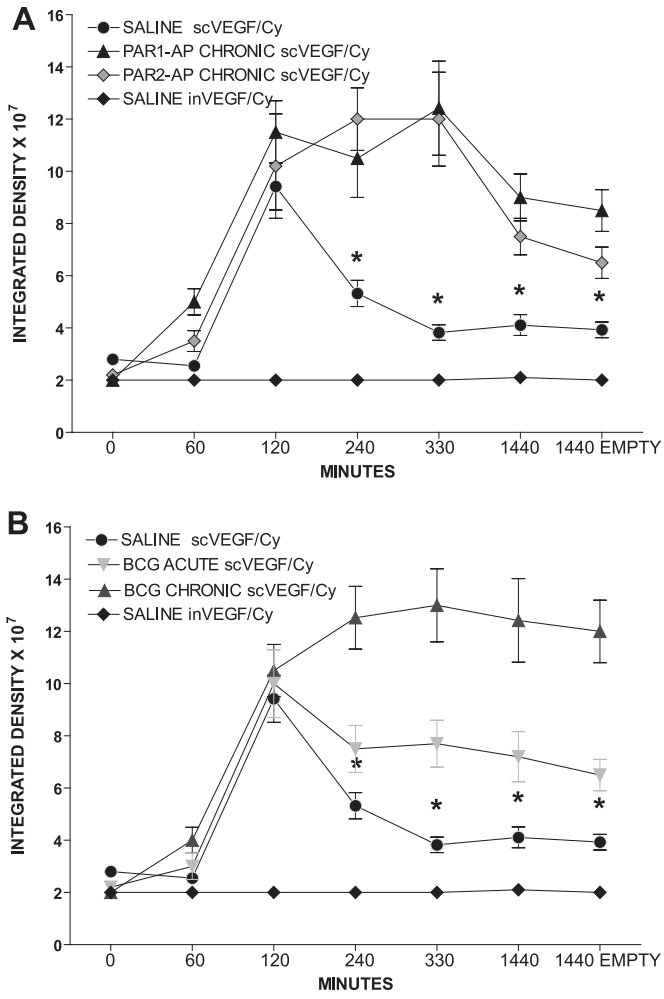

Fig. 2. Time-dependent variation in Cy5.5-integrated fluorescent density in regions of interest (ROI) in the urinary bladder. Integrated fluorescent density (IFD) $\times 10^7$ was obtained in PAR (*A*)- and BCG-treated (*B*) mice. All mice had intact skin during the scanning and the IFD was obtained in ROI of the bladder region, as illustrated by a red circle in Fig. 1, *A–F*. The IFD corresponds to the sum of the values of the pixels in the ROI, which were equivalent to the product of the area (in pixels) and mean gray value. Results are presented as means ± SE of 6 mice per point. *Statistically significant difference ($P <$ 0.05) between saline- and PAR-APs (*A*) or saline- and BCG-treated mice (*B*).

The PCR program consisted of one preincubation at 95°C for 2 min and 35 cycles at 95°C for 30 s, 55°C for 45 s, 72°C for 90 s, and 72°C for 5 min. All PCR reactions were performed with a Robocycler Gradient 96 with a heated lid (Stratagene, La Jolla, CA) in 50 μl of 1× PCR buffer, 1.5 mM $MgCl_2$, forward and reverse primers at 0.2 μM, 200 μM dNTP, and 1 U of *Taq* DNA polymerase (Invitrogen). Twelve microliters of the amplification mixtures were analyzed on a 2% agarose gel. GAPDH was used as positive control. Images of the PCR products were taken using the FluorChem HD digital darkroom (Alpha Innotech), and the area under the curve was quantified using Image J software (5).

Chromatin Immunoprecipitation and Quantitative Real-Time PCR-Based Assays of the Mouse Urinary Bladders

Additional female C57BL/6J mice (n = 20 per group) were anesthetized and instilled with the same substances described above. Isolated bladders were frozen and shipped to Genpathway (2) for querying the chromatin for gene transcription (Genpathway's TranscriptionPath Query assay) (31). Tissues were exposed briefly to formaldehyde for cross-linking of the proteins and DNA together, followed by sonication to fragment the DNA into pieces of ~300–500 bp. An antibody against RNA polymerase II (Abcam) was then used to precipitate the DNA transcriptome (37). The Ab-protein-DNA complexes were purified using beads coupled to protein A. The DNA was isolated from the complexes using a combination of heat to reverse cross-linking, RNase and proteases, and then purified using phenol extraction and EtOH precipitation. The final chromatin immunoprecipitation (ChIP) DNAs were then used as templates in quantitative PCR reactions using primer pairs specific for each gene of interest and designed using Primer 3 (3). The designed primers shared 100% homology with the target sequence, but no significant homology with other sequences and Q-PCR primer sequences for are given in Table 2. Quantitative PCR was carried out using *Taq* polymerase (iQ SYBR Green Supermix, Bio-Rad).

Q-PCRs were run in triplicate and the values were transferred into copy numbers of DNA using a standard curve of genomic DNA with known copy numbers. The resulting transcription values for each gene were also normalized for primer pair amplification efficiency using the Q-PCR values obtained with Input DNA (unprecipitated genomic DNA). Results are presented as Transcription Events Detected per 1,000 Cells for each gene tested.

Statistical Analysis of ChIP/Q-PCR Data and Image Analysis

The difference between two mean values was analyzed with an unpaired Student's t-test (GraphPad Prism software version 4.0; GraphPad Software, San Diego, CA). A nominal P value <0.05 was considered statistically significant.

Materials

scVEGF/Cy and inactivated scVEGF/Cy (inVEGF/Cy) were from SibTech (Brookfield, CT). PAR1-AP, PAR2-AP, and PAR4-AP were synthesized at the Molecular Biology Resource Facility, William K. Warren Medical Research Institute, OUHSC, as COOH-terminal amides, purified by high-pressure liquid chromatography, and characterized by mass spectroscopy. Peptide solutions were made fresh in PBS from powder.

RESULTS

NIRF Imaging of Urinary Bladder with scVEGF/Cy

In vivo imaging with scVEGF/Cy. We first addressed the question whether alterations in VEGF receptor activity induced by inflammation can be detected in live mice in real time. We reasoned that a useful tool for exploring VEGF receptor activity might be scVEGF/Cy fluorescent tracer whose binding and internalization are mediated by functionally active VEGF receptors (10). As a control, we employed, inVEGF/Cy, a fluorescent tracer based on scVEGF/Cy, but incapable of binding to VEGF receptors (10). Intravenous injection of inactivated tracer inVEGF/Cy in control mice instilled with saline did not lead to the appearance of fluorescence in lower abdominal area (Fig. 1*A*, red circle). In sharp contrast, intravenous administration of scVEGF/C in control mice led to accumula-

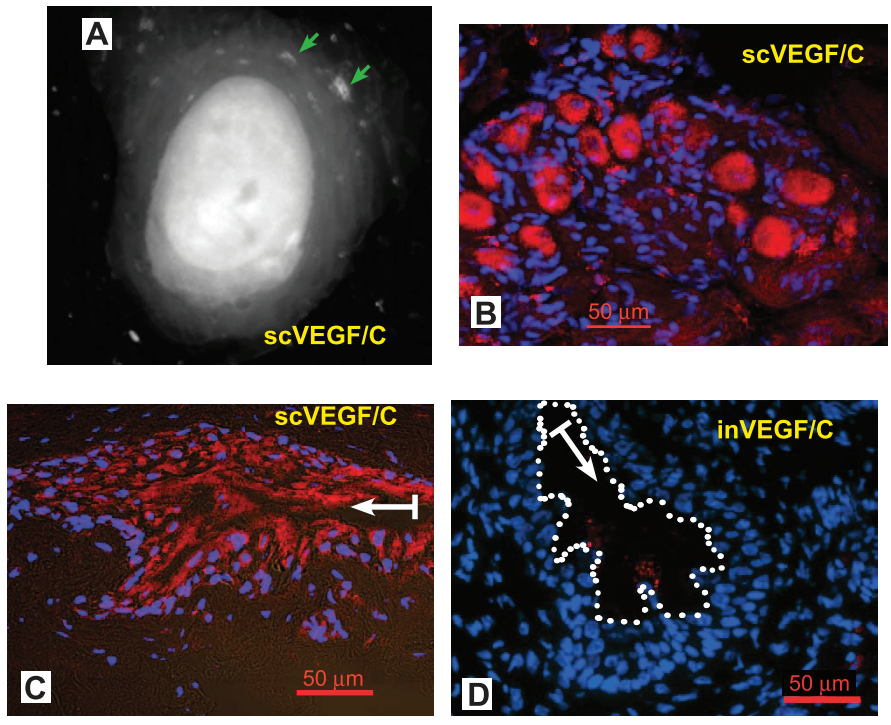

Fig. 3. Systemically administered scVEGF/Cy but not inVEGF/Cy accumulates in the urothelium and ganglia. These are representative images taken from a control mouse (instilled with saline) 24 h after intravenous administration of 100 μl of active tracer [scVEGF/Cy (*A*, *B*, and *C*)] and inactive tracer [inVEGF/Cy (*D*)], both at ~0.5 nmol. *A*: NIRF observed highlighting the urinary bladder 24 h following intravenous administration of scVEGF/Cy. *B*: uptake of scVEGF/Cy into intramural ganglia. *C*: representative confocal photomicrograph illustrating the uptake of the active tracer (scVEGF/Cy) in the bladder urothelium. *D*: illustrates the presence of inactive tracer (inVEGF/Cy) within the bladder lumen but not in urothelial cells (white arrow and dotted white line delimit the lumen).

tion of fluorescence in the lower abdominal area (Fig. 1*B*). The fluorescence was clearly elevated in mice inflamed chronically with PAR1-AP and injected with scVEGF/Cy (Fig. 1*C*). Figure 1, *D–I*, is representative photographs of the observed fluorescence in the lower abdominal region of a mouse chronically treated with PAR1-AP that was injected at *time 0* with scVEGF/Cy in the tail vein. Administration of scVEGF/Cy led to a time-dependent increase in NIRF in the mouse bladder (Fig. 1, *D–I*, ROIs in red circles). In this particular mouse, the fluorescence was detectable within minutes after scVEGF/Cy administration (Fig. 1*D*), while the peak fluorescence occurred at 120 min (Fig. 1*E*), and remained elevated throughout the study. Importantly, emptying the residual urinary content of the bladder did not significantly alter the intensity of fluorescence, indicating that the residual fluorescence corresponded to Cy5.5, which still remained within the bladder parenchyma (Fig. 1*I*). To establish that other abdominal organs do not contribute to observed fluorescence, additional mice have their abdomen opened and the gastrointestinal tract removed, to permit a better imaging of the pelvic area. Figure 1*J* is representative of the control group instilled with saline, Fig. 1*K* is representative of mice that received acute instillation with BCG, Fig. 1*L* was obtained from the group that received chronic BCG treatment, Fig. 1*M* represents chronic PAR1-AP, and Fig. 1*N* represents PAR-2AP chronic treatment group. Outside the urinary bladders (green arrows), fluorescence was observed at its highest concentration in the kidneys (red arrows), lymph sacs draining the lower abdomen (white arrows), and uterus (blue arrow). However, uptake in these organs was not detectable in intact mice, because of their location deeper in the abdominal cavity.

After establishing that fluorescence observed in the lower abdominal part of mice injected with scVEGF/Cy is due to uptake in the urinary bladder, we tested whether imaging in

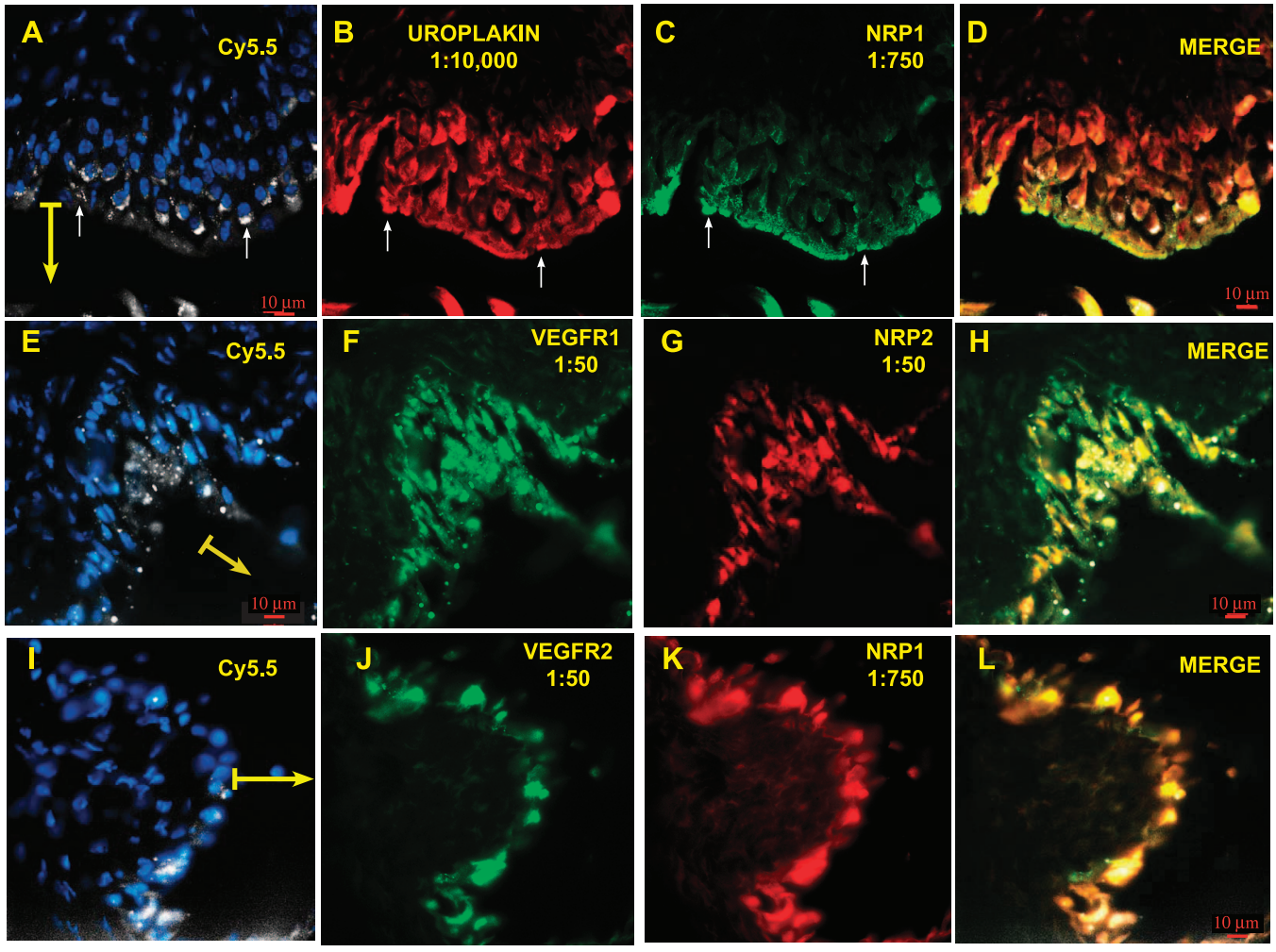

Fig. 4. scVEGF/Cy accumulation in the urothelium. Representative confocal photomicrographs of bladder urothelium isolated from mice that received systemic administration of the active tracer (scVEGF/Cy). *A*: colocalization of Cy5.5 (white) with DAPI (blue). *B*: expression of uroplakin (red), an urothelium-specific marker, by the bladder urothelial cells. *C*: expression of NRP1 in the mouse bladder urothelium. *D*: merged pictures of *A*, *B*, and *C* (DAPI was omitted for clarity) indicating the colocalization of NRP1 and Cy5.5 in uroplakin-positive urothelial cells. *E*: colocalization of Cy5.5 (white) with DAPI (blue). *F*: expression of VEGFR-1 (green) by the bladder urothelial cells. *G*: expression of NRP2 (red) in the mouse bladder urothelium. *H*: merged pictures of *E*, *F*, and *G* (DAPI was omitted for clarity) indicating the colocalization of VEGFR-1 and NRP2 in urothelial cells accumulating Cy5.5. *I*: colocalization of Cy5.5 (white) with DAPI (blue). *J*: expression of VEGFR-2 (green) by the bladder urothelial cells. *K*: expression of NRP1 (red) in the mouse bladder urothelium. *L*: merged pictures of *I*, *J*, and *K* (DAPI was omitted for clarity) indicating the colocalization of VEGFR-2 and NRP1 in urothelial cells accumulating Cy5.5. White arrows indicate cells coexpressing Cy5.5, uroplakin, and NRP1. Yellow arrows indicate the direction of bladder lumen.

intact animals in real time can be used for analysis of inflammation. In these experiments, we compared the time course of scVEGF/Cy uptake in mice treated with proinflammatory PAR1-AP, PAR2-AP, and BCG vs. control mice instilled with saline. We found similar kinetics and levels of tracer uptake in control and treated mice up to ~2 h postinjection (Fig. 2*A*). In contrast, mice treated intravesically with saline and injected with inVEGF/Cy presented only background fluorescence. However, the observed scVEGF/Cy fluorescence rapidly declined in control animals after a peak at 2 h postinjection. In contrast, such a decline was absent in animals chronically treated with inflammatory stimuli, and those mice displayed a larger increase and higher steady-state levels of fluorescence for far longer periods (Fig. 2*A*). Interestingly, a decline of fluorescence after 2 h postinjection was observed in mice treated with acute instillation of BCG (Fig. 2*B*). However, even in those mice the steady-state levels of retained fluorescence were significantly higher than in control mice (Fig. 2*B*).

Ex vivo localization of areas of enhanced scVEGF/Cy uptake. Since scVEGF/Cy tracer is internalized via receptor-mediated endocytosis and Cy5.5 is retained in the cells for at least several days, Cy5.5 fluorescence can be readily detected in tagged cells in harvested tissues (8–10). This enabled us to address the question of which anatomical structures in the bladder were involved in scVEGF/Cy uptake. Initial low-magnification fluorescent microscopy of the whole bladders from control mice revealed an elevated level of fluorescence in the areas of the lumen occupied by the urothelium (Fig. 3*A*). In addition, the bladder adventitia also presented some spots with a positive fluorescent signal (Fig. 3*A* green arrows). Cross-sections of the urinary bladders harvested from mice that received intravenous administration of inactive tracer (in-VEGF/Cy) presented low levels of Cy5.5 fluorescence exclusively in the bladder lumen (white arrow and white dotted line in Fig. 3*D* indicate the bladder lumen). In contrast, the urinary bladder harvested from mice that received intravenous administration of scVEGF/Cy demonstrated a clear accumulation of Cy5.5 in the urothelium (Fig. 3*C*). In addition to the urothelium, regions of adventitia that resembled ganglia also displayed the Cy5.5 fluorescence (Fig. 3*B*).

scVEGF/Cy Tags Urothelial Cells in the Urinary Bladder

Since the finding of scVEGF/Cy uptake in urothelium and ganglia-like structures was rather unexpected, we undertook a more detailed immunohistochemical analysis of scVEGF/Cy-tagged cells in bladders harvested from mice injected with this tracer. In these experiments, we used multicolor fluorescent confocal microscopy to explore colocalization of Cy5.5 fluorescence and immunofluorescent staining for specific markers, while DAPI was used for nuclear staining.

First, to validate the urothelial origin of scVEGF/Cy-tagged cells in the bladder lumen, we used a specific marker of urothelial cell differentiation, uroplakin, a protein component of the asymmetric unit membrane in urothelial cells (50). Analysis of immunostained sections indicated that uroplakin-positive cells occupy the lumen of the urinary bladder and that a significant number of those urothelial cells were tagged with

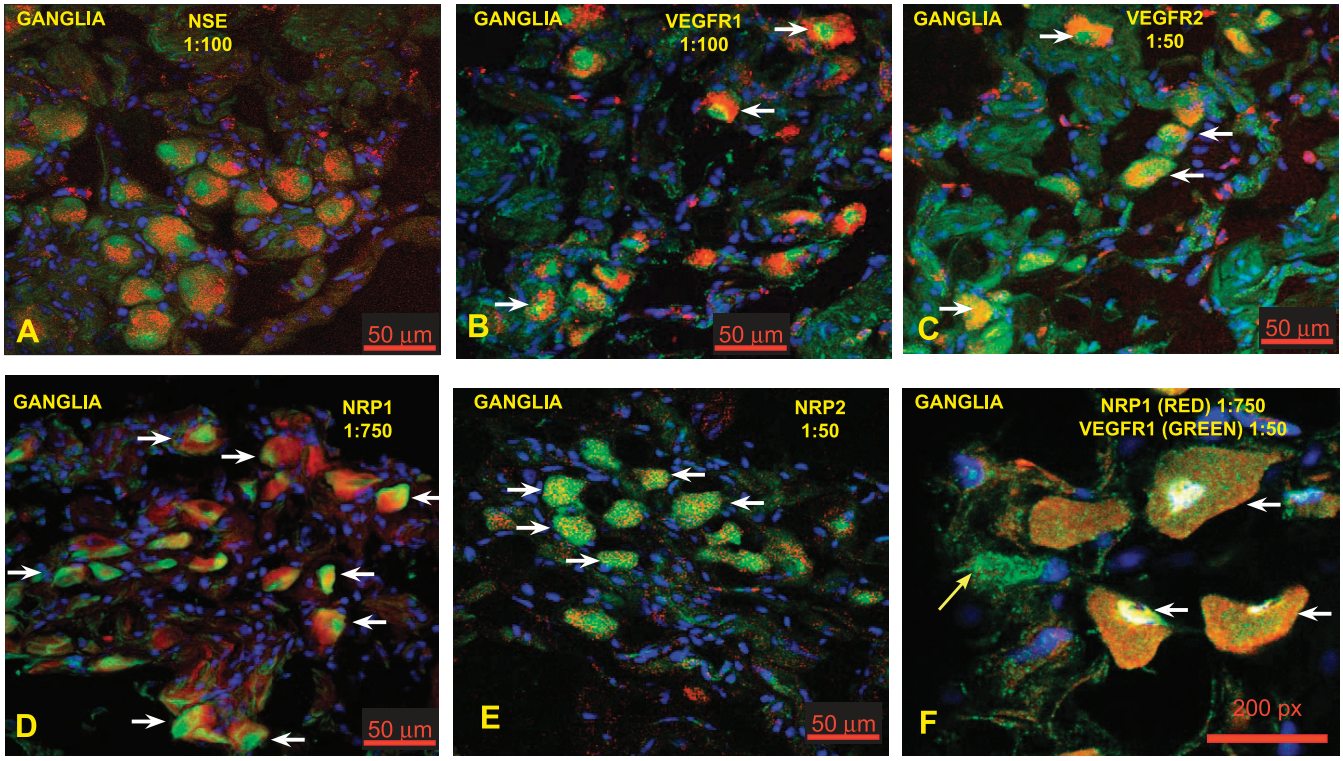

Fig. 5. scVEGF/Cy accumulation in the bladder ganglia. Representative confocal photomicrographs of bladder urothelium isolated from mice that received systemic administration of scVEGF/Cy. *A*: confocal projection of a representative area containing ganglia-like cells positively labeled with scVEGF/Cy and anti-NSE. *B*: colocalization of Cy5.5 and VEGFR-1. *C*: colocalization of Cy5.5 and VEGFR-2. *D*: colocalization of Cy5.5 and NRP1. *E*: colocalization of Cy5.5 and NRP2. *F*: colocalization of VEGFR1 and NRP1. Blue = DAPI and red = CY5.5. White arrows indicate cells coexpressing both Cy5.5 and the respective receptor being studied.

scVEGF/Cy (Fig. 4, *A* and *B*, are examples of colocalization of Cy5.5 and uroplakin-positive urothelial cells, as indicated by white arrows). In addition, Fig. 4, *C* and *D*, illustrates that uroplakin-positive urothelial cells are the ones expressing NRP1 and accumulating Cy5.5.

Since tagging with scVEGF/Cy required the presence of VEGF receptors, we tested whether VEGFR-1 and VEGFR-2 and its coreceptors (NRP1 and NRP2) were expressed in urothelial cells. Using histological sections stained for several markers (uroplakin and NRP-1, VEGFR-1 and NRP2, VEGFR-2 and NRP1), we found that tagged urothelial cells were positive for VEGFR-1 (Fig. 4*F*), VEGFR-2 (Fig. 4*J*), NRP-1 (Fig. 4*K*), and NRP-2 (Fig. 4*G*). We also determined colocalization of VEGFR-1 and NRP2 (Fig. 4*H*) and VEGFR-2 and NRP1 (Fig. 4*L*) in bladder urothelial cells.

scVEGF/Cy Tags Ganglia in the Urinary Bladder

To validate the neuronal origin of tagged cells in ganglia-like structures, we used a specific marker, neuronal-specific enolase (NSE), whereas DAPI was used for nuclear staining. We found that scVEGF/Cy-tagged cells in bladder ganglia-like structures were positive for NSE, indicating neuronal origin of those cells (Fig. 5*A*). Next, we determined which VEGF receptors were expressed in these cells and found that tagged cells in ganglia-like structures were immunostained for VEGFR-1 (Fig. 5*B*), VEGFR-2 (Fig. 5*C*), NRP1 (Fig. 5*D*), and NRP2 (Fig. 5*E*). We also determined that most of the ganglial cells express both VEGF-R1 and NRP1, as illustrated in Fig. 5*F*.

scVEGF/Cy Poorly Tags Endothelial Cells in the Urinary Bladder

Since VEGF receptors are typically expressed on vascular and lymphatic endothelial cells, we tested whether scVEGF/Cy tagged those cells in the bladder urothelium. Indeed, using immunostaining for pan-endothelial marker CD31, we found tagged cells among suburothelial CD31-positive cells (Fig. 6*A*). However, overall Cy5.5 fluorescence in such cells was modest compared with the urothelial cells (white dotted line). Certain Cy5.5 fluorescence was also detected in cells that were positive for lymphatic vessel marker LYVE-1 (Fig. 6*B*). Such cells were readily found in bladder adventitia, rather than in suburothelium where lymphatic vessels are rare (38). However, overall Cy5.5 fluorescence in LYVE-1-positive cells was modest (white arrows) compared with Cy5.5 fluorescence in ganglia (white dotted line in Fig. 6*B*).

Inflammation Increases the Number of scVEGF/Cy-Tagged Urothelial Cells

Since inflammation increased the steady-state levels of scVEGF/Cy uptake (Fig. 1) and urothelial cells were primarily responsible for scVEGF/Cy uptake in the urinary bladder, the next question to be answered was how inflammation increases the steady-state levels of scVEGF/Cy uptake. Using immunostained histological sections from control and treated mice injected with scVEGF/Cy, we determined the fraction of VEGF receptor-positive cells that were tagged with scVEGF. We found that in mice with bladder inflammation induced by chronic instillation of PAR1-AP and PAR2-AP, the fraction of either VEGFR-1- or VEGFR-2-positive cells that were tagged with scVEGF was two- to threefold higher than in control mice (Fig. 7*A*). Since VEGF receptors and NRPs colocalize in urothelium, it was not surprising to find that the fraction of scVEGF-tagged NRP1- and NRP2-positive cells also increased significantly (Fig. 7*A*). In contrast, the effects of inflammation induced by either chronic or acute BCG instillation were more

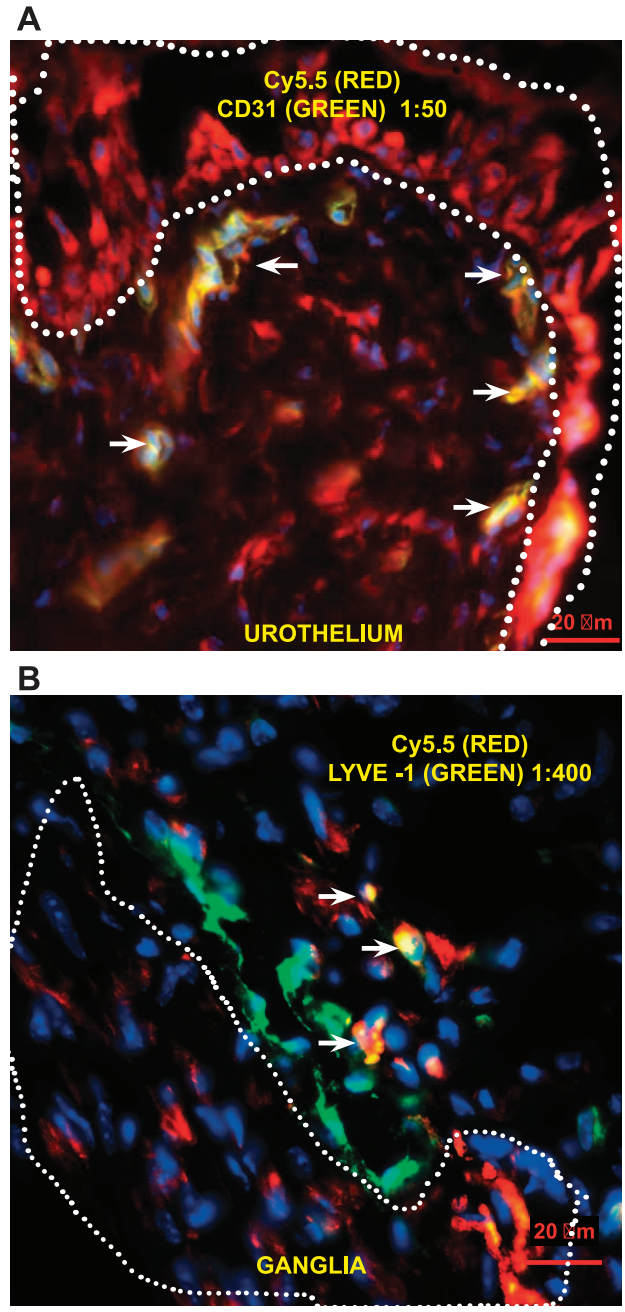

Fig. 6. scVEGF/Cy accumulates predominantly in urothelium and ganglia compared with blood and lymphatic vessels. *A*: colocalization of Cy5.5 and CD31-positive blood vessels in the bladder suburothelial layer. Note the intense accumulation of Cy5.5 in the urothelium (white dotted line) contrasting with scanty accumulation in CD31-positive blood vessels (white arrows). *B*: colocalization of Cy5.5 and LYVE-1-positive lymphatic endothelial cells in the bladder adventitia. Note the intense accumulation of Cy5.5 in LYVE-1-positive ganglial cells contrasting accumulation in LYVE-1-positive lymphatics (white arrows). Blue = DAPI and red = CY5.5. White arrows indicate cells coexpressing both receptors being studied.

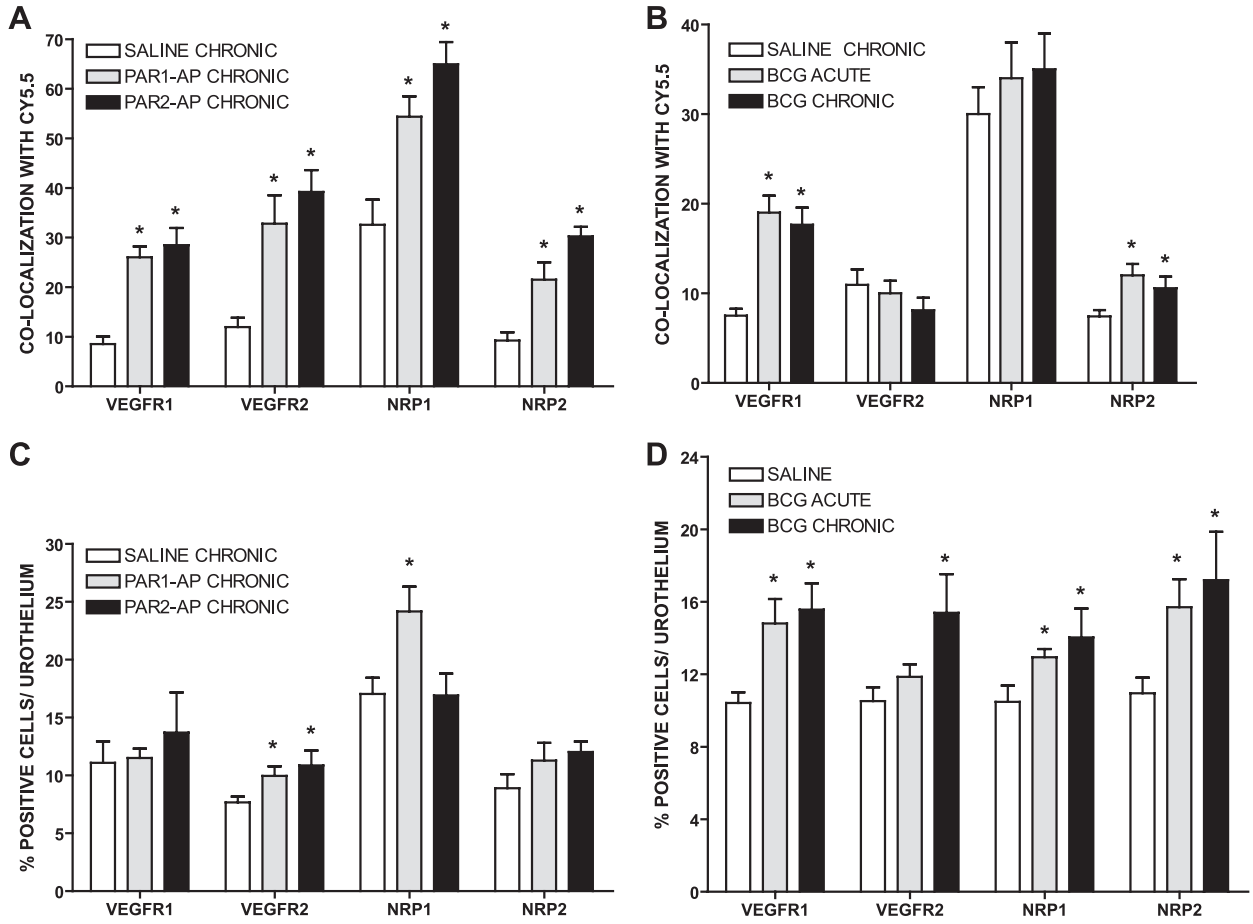

Fig. 7. Image analysis of the bladder urothelium. At least 6 random fields per cross-section ($n = 6$ per group) were visualized at ×20 magnification and used for image analysis that was performed with the NIS Elements Advanced Research 2.3 imaging software (6). The number of positive cells expressing a particular antibody was calculated as percent of the total area of the urothelium. Colocalization of one antibody and Cy5.5 was calculated by converting the area occupied by cells positive for the antibody into a ROI, and then calculating the percent of Cy5.5-positive cells within the ROI. Results are expressed as means ± SE. *Statistically significant difference ($P < 0.05$) between saline- and PAR-APs (*A* and *C*) or saline- and BCG-treated mice (*B* and *D*).

selective, enhancing the fraction of scVEGF/Cy-tagged only VEGFR-1- but not VEGFR-2- and NRP2- but not NRP1-positive cells (Fig. 7*B*). Taken together, this analysis indicated that inflammation resulted in the increase in the fraction of urothelial cells capable of receptor-mediated uptake of scVEGF/Cy tracer.

Next, we tested whether inflammation increased the fraction of scVEGF/Cy-tagged urothelial cells by recruiting additional cells to express VEGF receptors, or by enhancing accessibility of cells with preexisting VEGF receptors. To compare the fraction of urothelial cells expressing VEGF receptors, we determined the area occupied by marker-positive cells as a percentage of the total analyzed area on immunostained histological sections obtained from control and treated mice. We found that chronic instillation of mice with PAR1-AP and PAR2-AP did not affect the fraction of VEGFR-1-positive cells, but led to a small but statistically significant increase in VEGFR-2-positive cells (Fig. 7*C*). Furthermore, only PAR1-AP but not PAR2-AP increased the fraction of NRP1-positive cells and neither stimulus affected the fraction of NRP2-positive cells (Fig. 7*C*). We also compared the effects of acute and chronic BCG instillation and found that both treatments induced a small but statistically significant enhancement in the fraction of VEGFR-1-positive cells and that the chronic BCG also alters the fraction of VEGFR-2-, NRP1-, and NRP2-positive cells (Fig. 7*D*). Nevertheless, for all inflammatory stimuli, the increase in the fraction of receptor-positive cells was too small to explain the inflammation-induced two- to three-fold increase in the fraction of scVEGF/Cy-tagged cells among receptor-positive cells. We, therefore, hypothesized that inflammation increased accessibility of cells with preexisting VEGF receptors that led to higher scVEGF/Cy tracer accumulation.

Expression of NRP1 and VEGFR-1 by the Mouse Bladder Mucosa

The urothelium along with the submucosa was isolated from the detrusor muscle, the RNA was extracted, and PCR results indicate that the bladder urothelium/submucosa presents the message for NRP1, NRP2, VEGFR-1, and VEGFR-2 (Fig. 8).

ChIP-Q-PCR Assessment of VEGF Signaling in Bladder Inflammation

Inflammation-associated increase in the number of tracer-tagged urothelial cells might be due either to enhanced receptor expression or to the increase in the number of accessible cells

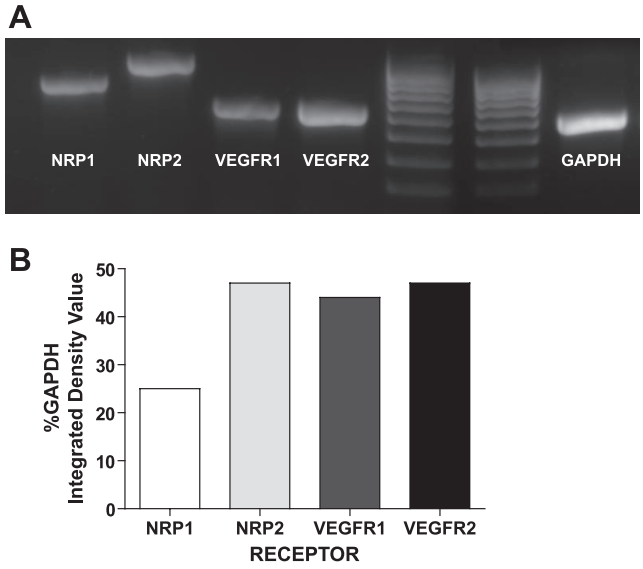

Fig. 8. PCR for detection of NRP1, NRP2, VEGFR-1, and VEGFR-2 message. *A*: photomicrograph of gels. *B*: area under the curve as quantified using Image J software (5). Primers used in this experiment are described in Table 2.

with preexisting receptors. To assess alterations in the receptor expression, we used chromatin immunoprecipitation (ChIP) combined with quantitative real-time PCR (Q-PCR), a method that uses the DNA transcriptome and, therefore, reflects transcription of active genes (37, 40, 41). Although we detected statistically significant inflammation-induced increase in the expression of some VEGF receptors and coreceptors, the changes were too small to be considered consequential (Fig. 9, *A–B*).

Expression of VEGFRs and NRPs by Human Urothelium

Since finding VEGF receptors and coreceptors on urothelial cells was rather unexpected and might be peculiar to mice, we investigated whether VEGFRs and NRPs are also present in human bladder urothelium. Using human bladder biopsies obtained from normal individuals and multicolor confocal fluorescent microscopy, we found intense immunostaining for VEGFR-1 (Fig. 10*A*), VEGFR-2 (Fig. 10*D*), NRP1 (Fig. 10*E*), and NRP2 (Fig. 10*B*) that was localized to urothelium and was absent in the deeper layers of the bladder. Finally, merged pictures indicate colocalization of VEGFR1 and NRP2 (Fig. 10*C*) and VEGFR2 and NRP1 (Fig. 10*F*).

DISCUSSION

Here, we present direct evidence that the majority of VEGF receptors and NRPs in normal and inflamed mouse urinary bladder, as well as in human bladder biopsies, is located on urothelial cells. By using molecular imaging and in vivo tagging with fluorescent scVEGF/Cy tracer, we established VEGF receptor-mediated accumulation of the tracer in the mouse urinary bladder in real time. Within the bladder wall, two main areas accumulated the tracer: the bladder urothelium and ganglia. As judged by colocalization of Cy5.5 fluorescence with immunofluorescent staining for lineage-specific markers, VEGF receptors and coreceptors in both structures, the tracer preferentially tagged urothelial and neuronal cells, but not vascular or lymphatic endothelial cells. Although there are several reports on immunohistochemical detection of VEGF receptors in urinary bladder (13, 14, 29), our findings in vivo, for the first time, identify these receptors as accessible and functionally active. Importantly, our findings that in vivo tagged urothelial cells display both VEGF receptors and NRP

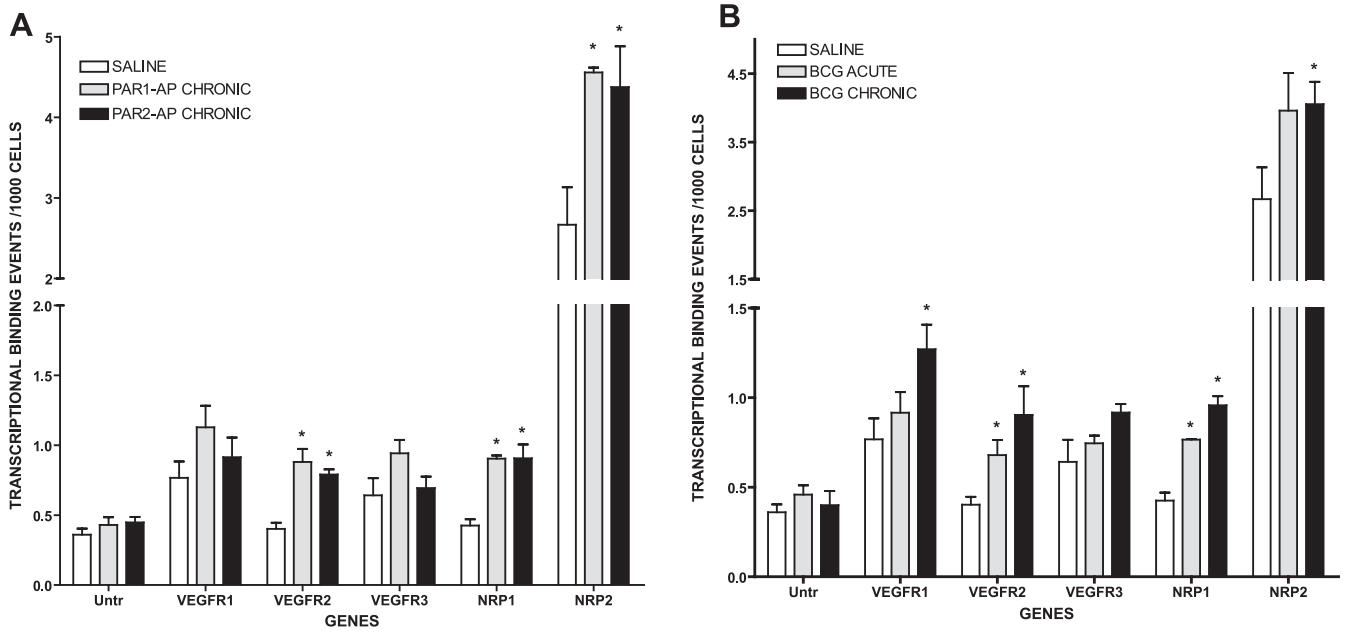

Fig. 9. Target validation by Q-PCR of chromatin immunoprecipitation (ChIP)-based assays. Mouse bladders were treated with saline, PAR-APs, or BCG (n = 20 per treatment group) and used for extraction of the chromatin (ChIP) and an antibody against RNA polymerase II (Abcam) was then used to precipitate the DNA transcriptome (37). Q-PCR was performed in triplicate using primer pairs described in Table 2. Results are presented as average and SE of transcription binding events detected per 1,000 cells. *Statistically significant difference ($P < 0.05$) between a specific gene between ChIPs isolated from PAR-APs and control-treated bladders (*A*) or BCG- and control-treated bladders (*B*). Untr, untranscribed region used as control.

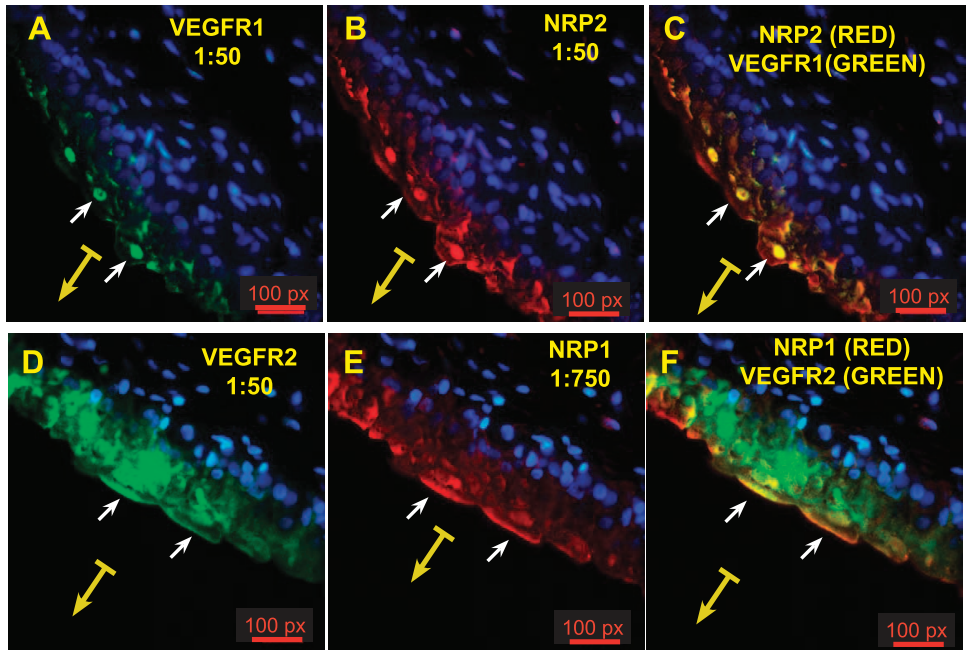

Fig. 10. Colocalization of VEGFR-1, VEGFR-2, NRP1, and NRP2 in human urothelium. Representative photomicrographs indicating that normal human urothelial cells express VEGFR-1 (*A*), VEGFR-2 (*D*), NRP2 (*B*), and NRP1 (*E*). *C*: illustrates the colocalization of VEGFR1 and NRP2. *F*: illustrates the colocalization of NRP1 and VEGFR-2 in the human urothelium. White arrows indicate cells coexpressing both receptors being studied and yellow arrows points to the bladder lumen.

coreceptors for $VEGF_{165}$ suggest that signal transduction can be induced by both $VEGF_{121}$ and $VEGF_{165}$ isoforms.

We also report here that bladder inflammation induced by various stimuli results in the enhanced scVEGF/Cy uptake in the bladder area. Analysis of tagged cells on histological cross-sections indicates that this effect is due primarily to two- to threefold increase in the number of urothelial cells capable of internalizing tracer in inflamed vs. normal bladder. Importantly, the increase in the number of tagged cells was significantly more pronounced than the enhancement in expression of VEGF receptors, as determined by immunohistochemistry and ChiP-Q-PCR. Although detailed mechanistic study will be required to account for the effects of inflammation, enhanced accessibility of urothelial cells might be explained by vasodilation and edema associated with bladder inflammation. It remains possible that inflammation could cause an increased nonspecific uptake of tracer (control or VEGF), although this may be unlikely based on previous findings with scVEGF/Cy (10).

The finding of functionally active VEGF receptors on urothelial and neuronal cells in the urinary bladder deserves speculations about the potential physiological functions of VEGF signaling in these cells. As with other nonendothelial cells (16, 19, 23, 30, 47), it can be suggested that urothelial VEGF receptors would enable VEGF to act as a survival factor under harsh conditions. Within this model, enhanced activity of VEGF receptors under inflammatory conditions would provide additional layer of protection for urothelium.

Although the main focus of this project is on the role of VEGF receptors in urinary bladder inflammation, our findings that NRPs are abundantly expressed in urothelial and neuronal cells in the urinary bladder are very intriguing. Therefore, we used normal human bladder biopsies to determine whether the human urothelium also expresses these receptors. Indeed, our results provide evidence of the presence and colocalization of VEGFR-1, VEGFR-2, NRP1, and NRP2 in the normal human urothelium. To date, there is a single report indicating a strong NRP2 mRNA expression in bladder muscle during development (18), and a report that in bladder cancer, NRP2 expression correlates with advanced tumor stage and grade (44). Interestingly, a substantial fraction of the NRP receptor is a glycosaminoglycan (GAG) modified with either heparan sulfate or chondroitin sulfate (45). Evidence was recently presented indicating that GAG modification of NRPs plays a critical role in modulating VEGF/NRP signaling (17, 22, 25, 28, 45), providing new insights into the role of neuropilins in the pathophysiology of bladder inflammation. In this respect, our finding of VEGF receptors and NRPs in the human urothelium raises the intriguing question of whether disorders that alter urothelium integrity and permeability such as interstitial cystitis, infection, and cancer can be diagnosed and/or treated via modulation of VEGF receptors and NRPs.

It can be argued that, besides scVEGF/Cy, other Cy5.5-containing fragments can be taken up by the urothelium. Since only functionally active scVEGF/Cy can get into cells in vivo, only functionally active fragments that retain the ability to bind to VEGF and NRP receptors were visualized. Since our test is functional, such fragments will not be distinguishable from intact scVEGF/Cy. Nevertheless, these fragments should retain the ability to bind to VEGFRs and NRPs as demonstrated in ex vivo experiments. Finally, the use of targeted tracer for whole animal NIRF followed by immunohistochemical analysis of cells tagged in vivo appears to be a promising approach to elucidating the mechanisms of normalcy and disease in the urinary bladder. Major advantages of this approach are *1*) opportunities to monitor uptake of the tracer in real time, and *2*) opportunities to identify cells with accessible and active receptors that bind and internalize the tracer in vivo. Since immunohistochemical analysis does not discriminate between "working" and "idle" receptors, in vivo tagging with appropriate tracer might significantly enrich our understanding of temporal and spatial distribution of signal transduction activity. Furthermore, since Cy5.5 is retained within the cell after targeting protein is degraded (24), there are opportunities

for longitudinal studies of tagged cells. In view of these advantages, it would be interesting to use a fluorescent endoscope for bladder examination with scVEGF/Cy tracer under conditions of inflammation and cancer.

Conclusion

We present evidence that functionally active and accessible VEGF receptors and NRPs are expressed in urothelium and neuronal cells in the mouse urinary bladder and that the accessibility of VEGF receptors and coreceptors is enhanced by inflammation. Our results strongly suggest that robust VEGF signaling occurs in bladder urothelium under normal and inflammatory conditions. These data were obtained using molecular imaging and receptor-mediated cell tagging in vivo with scVEGF/Cy fluorescent tracer, and we expect that this approach will be useful for the study of normal and diseased bladder physiology. In the long run, we expect that using scVEGF/Cy will complement the analysis of standard pathophysiological parameters and, therefore, permit the evaluation of VEGFR and neuropilin-targeted interventions for the treatment of inflammation.

GRANTS

This work was supported by National Institutes of Health Grants DK-55828-01 and DK-066101-01 (R. Saban), and Equipment Grant from Presbyterian Health Foundation C5033301 (R. Saban).

DISCLOSURES

J. Backer is a shareholder and an employee in SibTech, and M. Backer is an employee in SibTech.

REFERENCES

1. **Adobe photoshop CS3 extended.** http://wwwadobecom/products/photoshop/photoshopextended/.
2. **Genpathway.** http://wwwgenpathwaycom.
3. http://frodo.wi.mit.edu/cgi-bin/primer3/primer3_www.cgi.
4. http://www.the-aps.org/publications/journals/guide.htm#animals.
5. **Image software J.** http://rsbinfonihgov/ij/.
6. **NIS Elements.** http://wwwnis-elementscom/.
7. **Primer 3.** http://frodowimitedu/cgi-bin/primer3/primer3_wwwcgi.
8. **Backer MV, Backer JM.** Functionally active VEGF fusion proteins. *Protein Expr Purif* 23: 1–7, 2001.
9. **Backer MV, Gaynutdinov TI, Patel V, Bandyopadhyaya AK, Thirumamagal BT, Tjarks W, Barth RF, Claffey K, Backer JM.** Vascular endothelial growth factor selectively targets boronated dendrimers to tumor vasculature. *Mol Cancer Ther* 4: 1423–1429, 2005.
10. **Backer MV, Levashova Z, Patel V, Jehning BT, Claffey K, Blankenberg FG, Backer JM.** Molecular imaging of VEGF receptors in angiogenic vasculature with single-chain VEGF-based probes. *Nat Med* 13: 504–509, 2007.
12. **Bernard R.** *Hypothesis Testing for Correlation Coefficients.* Boston: PWS Publishers, 1990.
13. **Burgu B, McCarthy LS, Shah V, Long DA, Wilcox DT, Woolf AS.** Vascular endothelial growth factor stimulates embryonic urinary bladder development in organ culture. *BJU Int* 98: 217–225, 2006.
14. **Burgu B, Medina Ortiz WE, Pitera JE, Woolf AS, Wilcox DT.** Vascular endothelial growth factor mediates hypoxic stimulated embryonic bladder growth in organ culture. *J Urol* 177: 1552–1557, 2007.
15. **Campbell SC, Volpert OV, Ivanovich M, Bouck NP.** Molecular mediators of angiogenesis in bladder cancer. *Cancer Res* 58: 1298–1304, 1998.
16. **Carmeliet P, Storkebaum E.** Vascular and neuronal effects of VEGF in the nervous system: implications for neurological disorders. *Semin Cell Dev Biol* 13: 39–53, 2002.
17. **Cebe Suarez S, Pieren M, Cariolato L, Arn S, Hoffmann U, Bogucki A, Manlius C, Wood J, Ballmer-Hofer K.** A VEGF-A splice variant defective for heparan sulfate and neuropilin-1 binding shows attenuated signaling through VEGFR-2. *Cell Mol Life Sci* 63: 2067–2077, 2006.
18. **Chen H, Chedotal A, He Z, Goodman CS, Tessier-Lavigne M.** Neuropilin-2, a novel member of the neuropilin family, is a high affinity receptor for the semaphorins Sema E and Sema IV but not Sema III. *Neuron* 19: 547–559, 1997.
19. **Chintalgattu V, Nair DM, Katwa LC.** Cardiac myofibroblasts: a novel source of vascular endothelial growth factor (VEGF) and its receptors Flt-1 and KDR. *J Mol Cell Cardiol* 35: 277–286, 2003.
20. **Clavel G, Bessis N, Lemeiter D, Fardellone P, Mejjad O, Menard JF, Pouplin S, Boumier P, Vittecoq O, Le Loet X, Boissier MC.** Angiogenesis markers (VEGF, soluble receptor of VEGF and angiopoietin-1) in very early arthritis and their association with inflammation and joint destruction. *Clin Immunol Immunopathol* 124: 158–164, 2007.
21. **D'Andrea MR, Saban MR, Nguyen NB, Andrade-Gordon P, Saban R.** Expression of protease-activated receptor-1, -2, -3, and -4 in control and experimentally inflamed mouse bladder. *Am J Pathol* 162: 907–923, 2003.
22. **De Wit J, De Winter F, Klooster J, Verhaagen J.** Semaphorin 3A displays a punctate distribution on the surface of neuronal cells and interacts with proteoglycans in the extracellular matrix. *Mol Cell Neurosci* 29: 40–55, 2005.
23. **Deckers MM, Karperien M, van der Bent C, Yamashita T, Papapoulos SE, Lowik CW.** Expression of vascular endothelial growth factors and their receptors during osteoblast differentiation. *Endocrinology* 141: 1667–1674, 2000.
24. **Freeman MR, Schneck FX, Gagnon ML, Corless C, Soker S, Niknejad K, Peoples GE, Klagsbrun M.** Peripheral blood T lymphocytes and lymphocytes infiltrating human cancers express vascular endothelial growth factor: a potential role for T cells in angiogenesis. *Cancer Res* 55: 4140–4145, 1995.
25. **Fuh G, Garcia KC, de Vos AM.** The interaction of neuropilin-1 with vascular endothelial growth factor and its receptor flt-1. *J Biol Chem* 275: 26690–26695, 2000.
26. **Futami R, Miyashita M, Nomura T, Makino H, Matsutani T, Sasajima K, Tajiri T.** Increased serum vascular endothelial growth factor following major surgical injury. *J Nippon Med Sch* 74: 223–229, 2007.
27. **Halin C, Tobler NE, Vigl B, Brown LF, Detmar M.** VEGF-A produced by chronically inflamed tissue induces lymphangiogenesis in draining lymph nodes. *Blood* 110: 3158–3167, 2007.
28. **Heil M, Mitnacht-Krauss R, Issbrucker K, van den Heuvel J, Dehio C, Schaper W, Clauss M, Weich HA.** An engineered heparin-binding form of VEGF-E (hbVEGF-E). Biological effects in vitro and mobilizatiion of precursor cells. *Angiogenesis* 6: 201–211, 2003.
29. **Herrmann E, Eltze E, Bierer S, Kopke T, Gorge T, Neumann J, Hertle L, Wulfing C.** VEGF-C, VEGF-D and Flt-4 in transitional bladder cancer: relationships to clinicopathological parameters and long-term survival. *Anticancer Res* 27: 3127–3133, 2007.
30. **Ishida A, Murray J, Saito Y, Kanthou C, Benzakour O, Shibuya M, Wijelath ES.** Expression of vascular endothelial growth factor receptors in smooth muscle cells. *J Cell Physiol* 188: 359–368, 2001.
31. **Labhart P, Karmakar S, Salicru EM, Egan BS, Alexiadis V, O'Malley BW, Smith CL.** Identification of target genes in breast cancer cells directly regulated by the SRC-3/AIB1 coactivator. *Proc Natl Acad Sci USA* 102: 1339–1344, 2005.
32. **Macfarlane SR, Seatter MJ, Kanke T, Hunter GD, Plevin R.** Proteinase-activated receptors. *Pharmacol Rev* 53: 245–282, 2001.
33. **Mohamedali KA, Kedar D, Sweeney P, Kamat A, Davis DW, Eve BY, Huang S, Thorpe PE, Dinney CP, Rosenblum MG.** The vascular-targeting fusion toxin VEGF121/rGel inhibits the growth of orthotopic human bladder carcinoma tumors. *Neoplasma* 7: 912–920, 2005.
34. **Pavlovich CP, Kraling BM, Stewart RJ, Chen X, Bochner BH, Luster AD, Poppas DP, O'Donnell MA.** BCG-induced urinary cytokines inhibit microvascular endothelial cell proliferation. *J Urol* 163: 2014–2021, 2000.
35. **Rovina N, Papapetropoulos A, Kollintza A, Michailidou M, Simoes DC, Roussos C, Gratziou C.** Vascular endothelial growth factor: an angiogenic factor reflecting airway inflammation in healthy smokers and in patients with bronchitis type of chronic obstructive pulmonary disease? *Respir Res* 8: 53, 2007.
36. **Saban MR, Hellmich H, Nguyen NB, Winston J, Hammond TG, Saban R.** Time course of LPS-induced gene expression in a mouse model of genitourinary inflammation. *Physiol Genomics* 5: 147–160, 2001.
37. **Saban MR, Simpson C, Davis CA, Wallis G, Knowlton N, Frank MB, Centola M, Gallucci RM, Saban R.** Discriminators of mouse bladder response to intravesical Bacillus Calmette-Guerin (BCG). *BMC Immunol* 8: 6, 2007.

38. **Saban MR, Towner R, Smith N, Abbott A, Neeman M, Davis CA, Simpson C, Maier J, Mémet S, Wu XE, Saban R.** Lymphatic vessel density and function in experimental bladder cancer. *BMC Cancer* 7: 219, 2007.
39. **Saban R, D'Andrea MR, Andrade-Gordon P, Derian C, Dozmorov I, Ihnat MA, Hurst RE, Simpson C, Saban MR.** Mandatory role of proteinase-activated receptor 1 in experimental bladder inflammation. *BMC Physiol* 7: 4, 2007.
40. **Saban R, D'Andrea MR, Andrade-Gordon P, Derian C, Dozmorov I, Ihnat MA, Hurst RE, Simpson C, Saban MR.** Regulatory network of inflammation downstream proteinase-activated receptors. *BMC Physiol* 7: 3, 2007.
41. **Saban R, Simpson C, Davis CA, Dozmorov I, Maier J, Fowler B, Ihnat MA, Hurst RE, Wershil BK, Saban MR.** Transcription factor network downstream of protease activated receptors (PARs) modulating mouse bladder inflammation. *BCM Immunol* 8: 17, 2007.
43. **Saban R, Simpson C, Vadigepalli R, Memet S, Dozmorov I, Saban MR.** Bladder inflammatory transcriptome in response to tachykinins: neurokinin 1 receptor-dependent genes and transcription regulatory elements. *BMC Urol* 7: 7, 2007.
44. **Sanchez-Carbayo M, Socci ND, Lozano JJ, Li W, Charytonowicz E, Belbin TJ, Prystowsky MB, Ortiz AR, Childs G, Cordon-Cardo C.** Gene discovery in bladder cancer progression using cDNA microarrays. *Am J Pathol* 163: 505–516, 2003.
45. **Shintani Y, Takashima S, Asano Y, Kato H, Liao Y, Yamazaki S, Tsukamoto O, Seguchi O, Yamamoto H, Fukushima T, Sugahara K, Kitakaze M, Hori M.** Glycosaminoglycan modification of neuropilin-1 modulates VEGFR2 signaling. *EMBO J* 25: 3045–3055, 2006.
46. **Slobodov G, Feloney M, Gran C, Kyker KD, Hurst RE, Culkin DJ.** Abnormal expression of molecular markers for bladder impermeability and differentiation in the urothelium of patients with interstitial cystitis. *J Urol* 171: 1554–1558, 2004.
47. **Takahashi N, Seko Y, Noiri E, Tobe K, Kadowaki T, Sabe H, Yazaki Y.** Vascular endothelial growth factor induces activation and subcellular translocation of focal adhesion kinase (p125FAK) in cultured rat cardiac myocytes. *Circ Res* 84: 1194–1202, 1999.
48. **Troy T, Jekic-McMullen D, Sambucetti L, Rice B.** Quantitative comparison of the sensitivity of detection of fluorescent and bioluminescent reporters in animal models. *Mol Imaging* 3: 9–23, 2004.
49. **Visvanathan S, Wagner CL, Marini JC, Baker D, Gathany T, Han J, van der Heijde D, Braun J.** Inflammatory biomarkers, disease activity, and spinal disease measures in patients with ankylosing spondylitis after treatment with infliximab. *Ann Rheum Dis* 67: 511–517, 2008.
50. **Wu XR, Lin JH, Walz T, Haner M, Yu J, Aebi U, Sun TT.** Mammalian uroplakins. A group of highly conserved urothelial differentiation-related membrane proteins. *J Biol Chem* 269: 13716–13724, 1994.
51. **Wu XR, Manabe M, Yu J, Sun TT.** Large scale purification and immunolocalization of bovine uroplakins I, II, and III. Molecular markers of urothelial differentiation. *J Biol Chem* 265: 19170–19179, 1990.